Research Article

Shikang Qin, Qingfa Chen*, Qinglin Chen, and Fuyu Zhao

Correlation between ore particle flow pattern and velocity field through multiple drawpoints under the influence of a flexible barrier

https://doi.org/10.1515/geo-2019-0043
Received May 14, 2018; accepted Apr 29, 2019

Abstract: By means of similar tests, the stope room is scaled and the process of multiple-drawpoint ore drawing under the influence of a flexible barrier is simulated by the marking particle method. Based on the experimental phenomena and data, the shape of the barrier, the draw column, and the numerical relations for the discharge between each drawpoint are analysed. The velocity equation for ore particles flowing through multiple drawpoints is established and the relationship between ore particle flow properties and velocity fields is found. Finally, the following results are derived: 1) For each layer, the morphology of marked particles is similar to that of vertical velocity. The particles are quasi-linear in the upper part of the model and wavy in the lower part. The amplitude increases with decreasing height. 2) The distribution of thirteen concentric points of horizontal velocity in each layer illustrate that the ore particles drawn from each drawpoint are from the centreline between it and the adjacent drawpoint. 3) The barrier and the marked particles are at the lowest sag points at the top of the number two and number six drawpoints (close to the model's side wall) because of the combination of vertical velocity and horizontal velocity.

Keywords: ore particle; the flexible barrier; multiple drawpoints; flow pattern; velocity field

1 Introduction

Under the guidance of green, no-waste mining [1–4], the idea of "synchronous filling" in mining technology was proposed and the method of mass draw and synchronous filling with no-top-pillar shrinkage stoping (i.e., synchronous filling mining) was invented by the author in 2010 [5]. In the new mining method, which is based on the traditional shrinkage method, a flexible barrier is laid on the surface of an ore pile before drawing the ore. In the process of drawing, filling materials are filled into the stope room through the return airway in a timely fashion and the filling materials and ore particles sink synchronously and uniformly [6]. The ore particles are drawn under the influence of a flexible barrier which does not come into direct contact with the waste rocks. Accordingly, there is no ore loss or dilution in the ore particles drawn. The flow behaviour of the ore particles in the new mining method is a breakthrough over traditional draw theories. Because of the existence of the barrier, the new mining method breaks through the description category of traditional draw theory; therefore, further research is needed. Thus far, the author has completed research on the flow behaviour of the ore particles under the influence of a flexible barrier and the evolution law for the flexible barrier [7–9]. In order to further understand the flow properties of ore particles and the mechanism of the synchronous filling stoping method, it is necessary to study the correlation between the flow patterns and velocity fields of ore particles under the influence of a flexible barrier.

The motion condition of each particle in the stope room can be determined by the distribution of its velocity field; accordingly, the motion trail of ore particles and the morphology of the draw column can be determined by this velocity field, which can provide a theoretical basis for stope design and stope structure parameter optimization. Over the years, substantial research has been conducted in this area. Rustan [10] pointed out the importance of studying the velocity field of ore particles for mining engineering applications. Later, Brown [11] and Kuchta [12] studied the velocity fields of ore particles in the caving method. Subsequently, Tao *et al.* [14] improved the method of determining the bulk vacancy diffusion coefficient in the drawing process based on a kinematics model and preliminarily

***Corresponding Author: Qingfa Chen:** School of Resources, Environment and Materials, Guangxi University, Nanning 530004, China; Email: gxumining@163.com
Shikang Qin, Qinglin Chen, Fuyu Zhao: School of Resources, Environment and Materials, Guangxi University, Nanning 530004, China

established the flow velocity equation for ore particles in two- and three-dimensional space.

The above studies provide new ideas for further development of draw theory, but these studies focused on the flow laws and velocity fields of ore and rock under the condition of a single drawpoint; few studies have considered the condition of more complex, multiple drawpoints, and the influence of flexible barriers has not been considered. Therefore, based on classical draw theory and considering the influence of a flexible barrier, this study examines the flow patterns and the velocity field equations of ore particles and the correlation between them with multiple drawpoints. This further promotes research on the method of mass draw and synchronous filling with no-top-pillar shrinkage stoping.

2 Experimental model and method

2.1 Experiment model

In order to study the flow law for ore particles in the synchronous filling mining method, based on the similarity principle [15–17], the similarity model shown in Figure 1 was designed using the average stope room size of the Tongkeng mine, Guangxi, China as a reference [7]; the similarity ratio was 25:1.

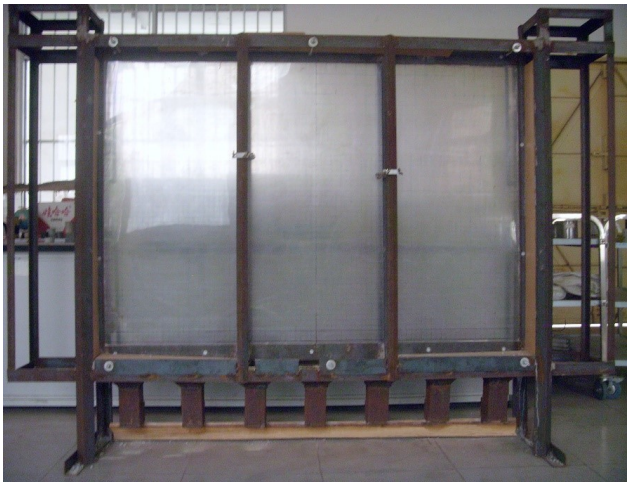

Figure 1: Physical test model.

The length of the ore block in the model was 200 cm, the stage height was 160 cm, and the thickness was 24 cm. The spacing between drawpoints was 24 cm, the size of the drawpoint was 8 cm × 8 cm and the serial number from left to right was one to seven. The frame of the model material consisted mainly of angled steel, flat steel, and metal plates. Two PC plates were placed on either side of the model. The front PC plate was drawn into movable 2 cm × 2 cm cells. The rear PC plate was divided into three equal pieces.

2.2 Experimental method

Ore from Tongkeng mine, Guangxi, China was broken according to the above similarity ratio and 1000 ore particles were selected manually and colored with dye as marker particles. The ore particle size was normally distributed with an average lumpiness of 2 cm. The loading bulk density of ore particles was 1.53 kg/L, the humidity was 0.14%, the natural rest angle was 35.8°, and the internal friction angle was 41.5°. The marked particles with a diameter of 2 cm were laid in the model in an orderly manner at a certain height interval. After the entire model was filled, the pre-purchased silicon rubber with a thickness of 2 mm was evenly spread over the surface of the ore particles to simulate a barrier. A camera was set up in front of the model and its lens was adjusted to focus on the centre of the PC plate so as to record the model data in the test.

During the test, a wood baffle strip was vibrated up and down and the ore particles were drawn gently. To simulate a synchronous filling process, waste rocks were filled into the model in a timely fashion while the ore particles were drawn. After a certain number of particles were drawn, the ore particles drawn from each drawpoint were weighed. The number of marked particles from each corresponding drawpoint and the data captured by the camera were recorded.

3 Flow pattern of ore particles through multiple drawpoints

3.1 Experimental phenomena

During the initial stage of ore drawing, the barrier is in close contact with the ore surface and the two components move gently downward together. With the continuous discharge of ore particles, the marked particles in the upper part move downward in a quasi-linear manner, the marked particles in the lower part moved down in an undulating manner, and the amplitude of the marked particles increases as they move downward. The experimental phenomena observed over several stages are shown in Figure 2.

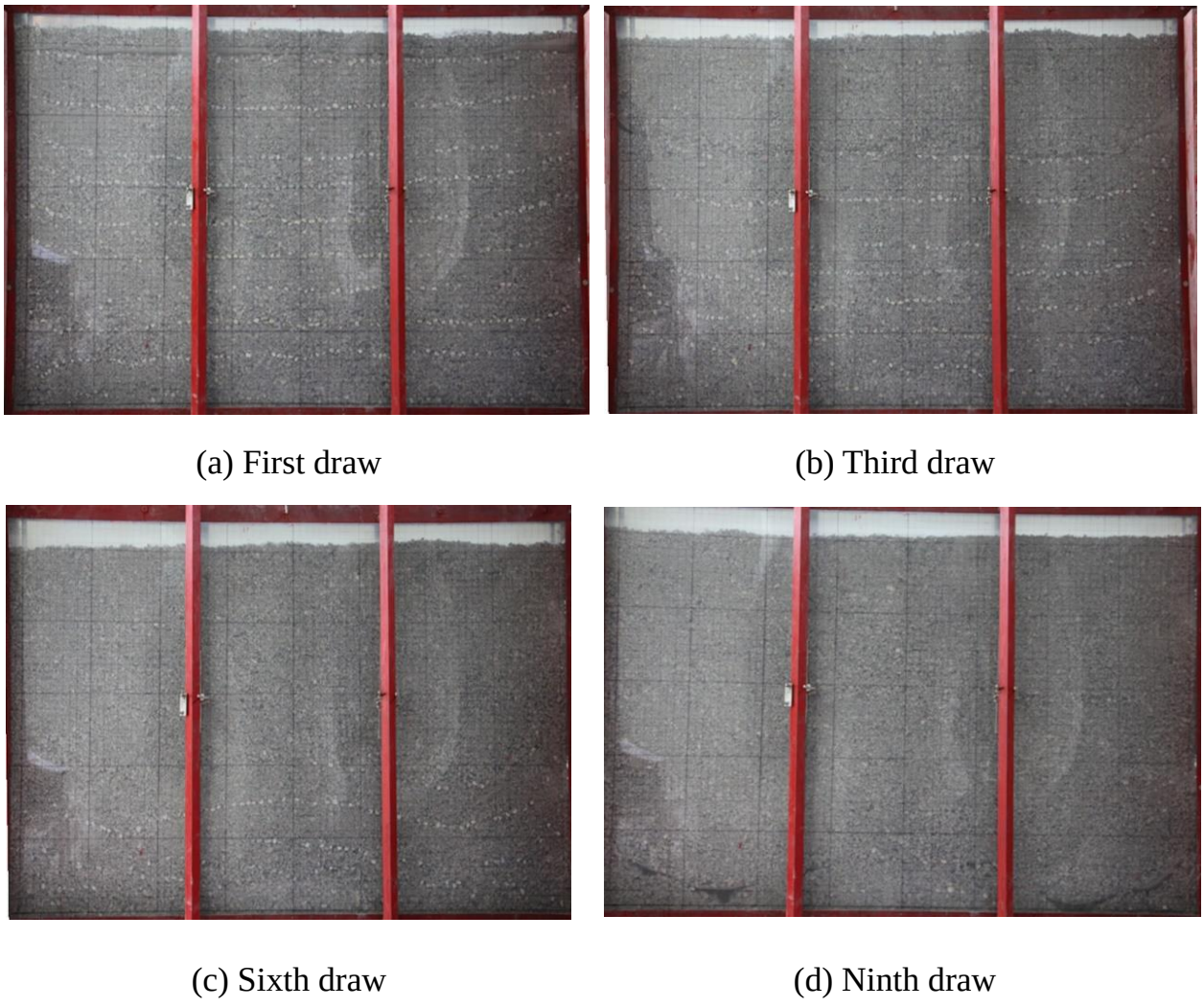

Figure 2: Experiment phenomena in different stages.

When the number of particles drawn reaches a certain value, a gap between the barrier and the ore surface begins to appear. As the number of particles drawn increases, the gap grows larger. When no particles are drawn from the drawpoints, the barrier is suspended on the drawpoints in a wavy shape.

3.2 Morphology evolution law for the barrier interface

During the test, every time a certain amount of ore particles was drawn, the descent depth h of the barrier was measured and the location of the barrier was recorded by a high-speed camera. The representative interface morphology curve of the barrier was drawn on a single graph and the dynamic evolution process of the interface of the barrier can be clearly seen, as shown in Figure 3.

The barrier was horizontal before the draw started; after opening the drawpoint, the barrier sank and bent gradually as the particles in the model were constantly drawn under the combined action of the load caused by backfilling waste particles and the particle flow field. When the discharged quantity reached a certain value, the barrier began to appear uneven. The concave–convex characteristics became more obvious as the ore particles continued to be drawn. The lowest sag points of the barrier were at the top of the number two and number six drawpoints close to the side wall of the model. The barrier separated from the ore surface in some places. The barrier was suspended in an undulating shape above each drawpoint when the ore was not being drawn. There was no residue of pure ore

Table 1: Statistical results for accumulated mass drawn (Q) and draw column height (H) at each drawpoint in the test.

Drawpoint no.		1	2	3	4	5	6	7
		Accumlated mass drawn/kg						
Draw Column height /cm	21.4	3.15	3.65	3.05	3.4	3.35	3.25	2.55
	36.4	11.75	12.1	11.15	10.7	10.65	12.2	11.25
	46.4	15.4	16.5	15.5	14.9	15.05	17.1	16.5
	56.4	21.45	24	21.05	20.45	20.9	23.75	22.9
	66.4	27.55	30.55	26.65	26.1	26.95	30.95	27.45
	76.4	32	36.35	31.75	31.2	31.75	36.45	32.65
	86.4	37.75	42.15	38.25	36.65	37.7	43.35	39.35
	94.4	40.85	45.6	41.25	40.45	40.9	46.9	42.85
	108.4	48.95	53.25	49.6	47.85	48.65	54.75	51.25
	120.4	57.5	61.45	61.6	58.05	59.35	62.45	60.95

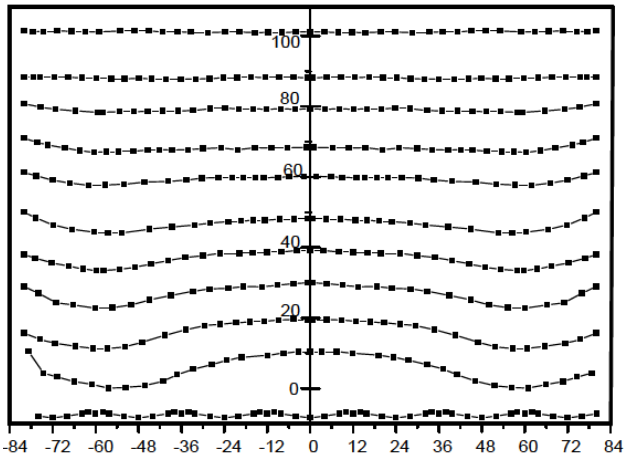

Figure 3: Morphology evolution process for the barrier interface.

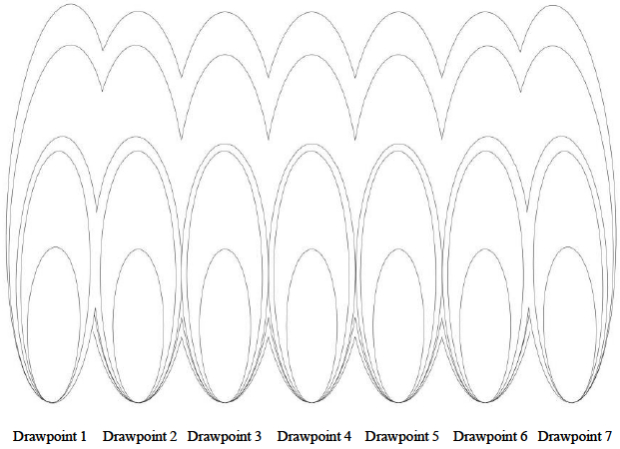

Figure 4: Morphology evolution of the draw column with multiple drawpoints.

along the ridges of the model because of the presence of the barrier.

3.3 Morphology evolution law for the draw column interface

To illustrate the shape of the draw column, the marked particles were sketched along the original coordinates and the boundaries of the marked particles drawn were connected smoothly. The shape of the draw column was then outlined [18–20]. The morphological evolution of the draw column was as shown in Figure 4.

As shown in Figure 4, the morphology of the draw column at each drawpoint still maintained an approximately ellipsoid shape similar to that observed for a single drawpoint. Furthermore, the ellipsoid expanded as more particles were drawn. The particles drawn from each drawpoint intersected to a certain extent and most of the ore particles drawn from each drawpoint came from the centreline between it and the adjacent drawpoint. Because of the influence of the side wall, the draw columns of drawpoints one and seven were slightly biased towards the centre of the model, consistent with the law of side ore drawing.

3.4 Relationship between draw column height and accumulated mass drawn

Based on the number of marked particle layers in the test, a total of ten measurements of the mass drawn were taken. The statistical results for the accumulated mass drawn (Q) and the height of the draw column (H) at each drawpoint in the test are shown in Table 1.

The data in Table 1 are plotted in Figure 5, showing how the accumulated mass drawn (Q) changes with the height of the draw column (H).

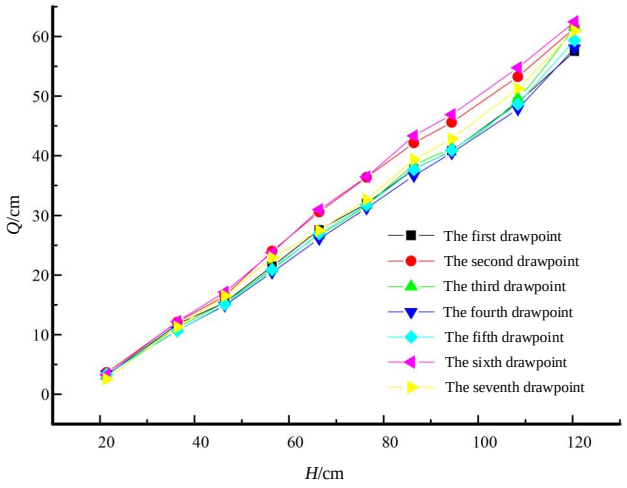

Figure 5: Broken-line graph showing the relationship between accumulated mass drawn (Q) at each drawpoint and draw column height (H).

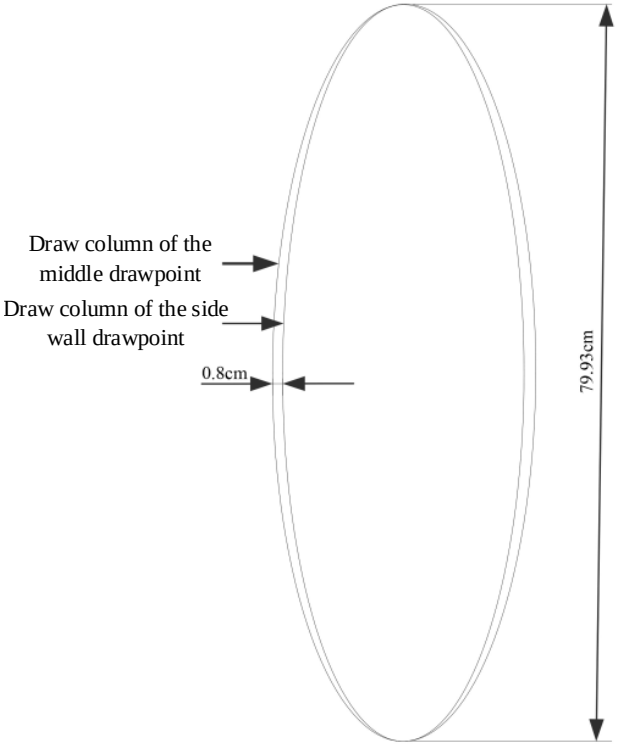

Figure 6: Comparison of the draw column of the middle drawpoint and the side wall drawpoint.

From Figure 5, we see that the mass drawn through each drawpoint grew exponentially at first and increased linearly thereafter. The mass drawn was slightly different for each of the seven drawpoints. Among the drawpoints, the least mass drawn was from the first drawpoint while the most was from the sixth drawpoint. The difference in the mass drawn of these two drawpoints was 4.95 kg. The mass drawn of the second, third, and seventh drawpoints were consistent at approximately 61 kg each. The masses drawn from the fourth and fifth drawpoints were moderate at approximately 59 kg each. Although the masses drawn at the first and seventh drawpoints were slightly less than at the other two groups of symmetrical drawpoints, these drawpoints still maintained a combined discharge level of approximately 120 kg.

To summarize, the boundary drawpoint had little influence on the mass drawn at all other drawpoints. The mass drawn at each drawpoint was essentially the same per unit time in this test, within an allowable range of error. This was consistent with results of previous research, which showed that the volume of particles drawn per unit time from a drawpoint of a certain diameter is constant [21].

4 Velocity field of ore particles through multiple drawpoints

4.1 Determination of particle flow parameters

The movement of particles in any part of the drawing process can be determined by the velocity equation. This equation is a fundamental equation used in the study of other physical phenomena. Therefore, the speed of the particles is an important parameter characterizing their movement. In the draw experiment using multiple drawpoints to simulate the synchronous filling shrinkage stoping method, the particle flow velocity was the superposition of the particle flow velocity induced by each drawpoint and the mass drawn through each drawpoint per unit time was equal; therefore, the flows of ore particles through the drawpoints interacted with each other but were also independent. For the five central drawpoints that were situated away from the side wall, the effect of the side wall could be ignored. Although the particles at the first and seventh drawpoints were located near the side wall, the distance between the centre of the model and the side wall of the drawpoint was 12 cm and the side wall was at a 90° angle. In addition, there was no significant difference in the morphology of the draw columns in this experiment, as shown in Figure 6. Therefore, flow parameters of the particles at the first and seventh drawpoints can be approximated using the parameters of the other five drawpoints when drawn independently. The particle speed in this experiment was calculated using the plane model. The velocity of moving par-

ticles at each drawpoint can be expressed using stochastic medium theory [22–25].

The velocity equation for particles from the second to the fifth drawpoints is

$$\begin{cases} v_z = -\frac{q}{\pi\beta_s z^{\alpha_s}} \exp\left(-\frac{r^2}{\beta_s z^{\alpha_s}}\right) \\ v_r = -\frac{\alpha_s q r}{2\pi\beta_s z^{\alpha_s+1}} \exp\left(-\frac{r^2}{\beta_s z^{\alpha_s}}\right) \end{cases} \tag{1}$$

where α_s and β_s are the flow parameters of particles when drawn independently; q is the mass drawn per unit time; r is the abscissa of the released particles and z is the ordinate of the released particles; v_z is the vertical velocity and v_r is the horizontal velocity.

The flow velocity equation for particles from the first and seventh drawpoints is

$$\begin{cases} v_z = -\frac{q}{\pi\beta_s A z^{\alpha_s}} \exp\left(-\frac{r^2}{\beta_s z^{\alpha_s}}\right) \\ v_r = -\frac{\alpha_s q r}{2\pi\beta_s A z^{\alpha_s+1}} \exp\left(-\frac{r^2}{\beta_s z^{\alpha_s}}\right) \end{cases} \tag{2}$$

where A is the shear coefficient of the end wall $A = \frac{1}{2} + \frac{1}{\sqrt{\pi}} \int_0^{\frac{12}{\sqrt{\beta_s z^{\alpha_s}}}} \exp(-\mu^2) d\mu$ and other symbols are as described earlier.

To determine the flow parameters of the particles when drawn independently, an ore draw experiment through a single drawpoint was designed. Only drawpoint four was opened for this experiment and the boundary test data of the draw column was read when the release height was 123 cm. The data are shown in Table 2.

Table 2: Boundary data table for the draw column under the influence of a flexible barrier.

r/cm	0	10.68	16.42	16.91	18.07
z/cm	126.54	114.24	92.18	81.94	56.27

The formula for the draw column in a plane could be obtained using random medium theory. Using this theory, we found that $\alpha_s = 1.453$, $\beta_s = 0.465$, and the correlation coefficient was 0.996.

4.2 Study of the superposition effect of velocity

The lowest point of the draw column in drawpoint 4 was used as the origin of the coordinates. The line that passes vertically through the bus of the draw column was designated as the z-axis and the line that points horizontally to the right was considered as the r-axis. This Cartesian coordinate system is shown in Figure 7.

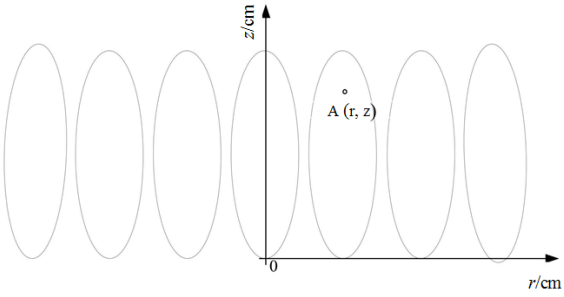

Figure 7: Cartesian coordinate system for the model.

The other six speed equations were adjusted appropriately to be consistent with the Cartesian coordinate system as shown in Figure 7. The velocity at any point in the model would be a superposition of the velocity at the seven drawpoints, in which case the vertical and horizontal velocities can be expressed as follows:

Vertical velocity:

$$\begin{aligned} v_z = & -\frac{q}{\pi\beta_s z^{\alpha_s}} \exp\left(-\frac{r^2}{\beta_s z^{\alpha_s}}\right) \\ & - \frac{q}{\pi\beta_s z^{\alpha_s}} \exp\left(-\frac{(r-24)^2}{\beta_s z^{\alpha_s}}\right) - \frac{q}{\pi\beta_s z^{\alpha_s}} \exp\left(-\frac{(r-48)^2}{\beta_s z^{\alpha_s}}\right) \\ & - \frac{q}{\pi\beta_s z^{\alpha_s}} \exp\left(-\frac{(r+24)^2}{\beta_s z^{\alpha_s}}\right) - \frac{q}{\pi\beta_s z^{\alpha_s}} \exp\left(-\frac{(r+48)^2}{\beta_s z^{\alpha_s}}\right) \\ & - \frac{q}{\pi\beta_s A z^{\alpha_s}} \exp\left(-\frac{(r+72)^2}{\beta_s z^{\alpha_s}}\right) \\ & - \frac{q}{\pi\beta_s A z^{\alpha_s}} \exp\left(-\frac{(r-72)^2}{\beta_s z^{\alpha_s}}\right) \end{aligned} \tag{3}$$

Horizontal velocity:

$$\begin{aligned} v_r = & -\frac{\alpha_s q r}{2\pi\beta_s z^{\alpha_s+1}} \exp\left(-\frac{r^2}{\beta_s z^{\alpha_s}}\right) \\ & - \frac{\alpha_s q (r-24)}{2\pi\beta_s z^{\alpha_s+1}} \exp\left(-\frac{(r-24)^2}{\beta_s z^{\alpha_s}}\right) \\ & - \frac{\alpha_s q (r+24)}{2\pi\beta_s z^{\alpha_s+1}} \exp\left(-\frac{(r+24)^2}{\beta_s z^{\alpha_s}}\right) \\ & - \frac{\alpha_s q (r-48)}{2\pi\beta_s z^{\alpha_s+1}} \exp\left(-\frac{(r-48)^2}{\beta_s z^{\alpha_s}}\right) \\ & - \frac{\alpha_s q (r+48)}{2\pi\beta_s z^{\alpha_s+1}} \exp\left(-\frac{(r+48)^2}{\beta_s z^{\alpha_s}}\right) \\ & - \frac{\alpha_s q (r-72)}{2\pi\beta_s A z^{\alpha_s+1}} \exp\left(-\frac{(r-72)^2}{\beta_s z^{\alpha_s}}\right) \\ & - \frac{\alpha_s q (r+72)}{2\pi\beta_s A z^{\alpha_s+1}} \exp\left(-\frac{(r+72)^2}{\beta_s z^{\alpha_s}}\right) \end{aligned} \tag{4}$$

Based on Equations (3) and (4), the vertical and horizontal velocities of the ore particles in each layer are

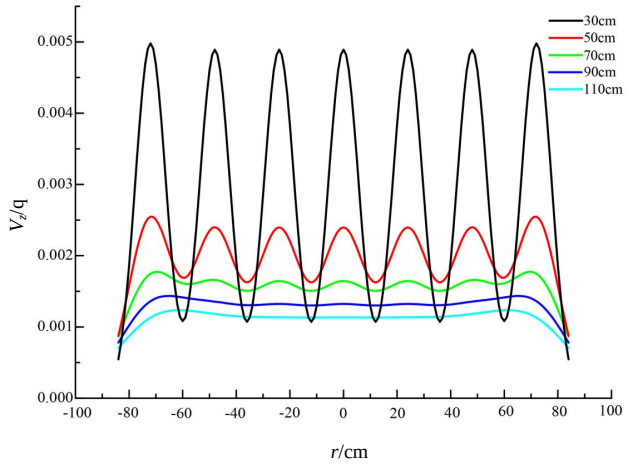

Figure 8: Vertical velocity of the ore particles in each layer.

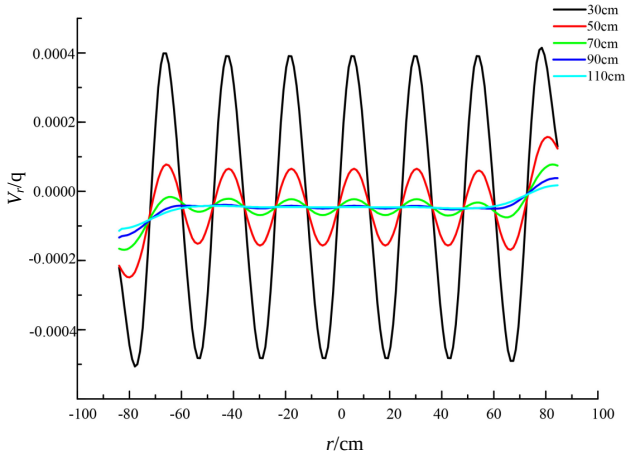

Figure 9: Horizontal velocity of the ore particles in each layer.

shown in Figures 8 and 9 when the draw amount is q per unit time at each drawpoint.

Figure 8 shows that the velocity fluctuations are highest at the bottom of the model. The fluctuations become smaller toward the top, ultimately tending toward a straight line. The velocity at the centre of both the No.1 and No. 7 drawpoints was greater than at the other five drawpoints owing to the influence of the side wall, resulting in the best ore liquidity. The velocity near the side wall was the lowest throughout the model and the liquidity of the corresponding particles was the worst.

Figure 9 shows that the horizontal velocity of each layer in the model is a sine curve and the origin of all vibrations is at $v = 0$. Below $v = 0$, the velocity is negative, indicating that the particle's velocity points to the right, while it points to the left above $v = 0$. There are thirteen concentric points in the Figure 9; most of them aggregate near the centreline of each pair of drawpoints or the centreline of each drawpoint except at the point where $r = 0$. The velocity where $r = 0$ is always equal to zero.

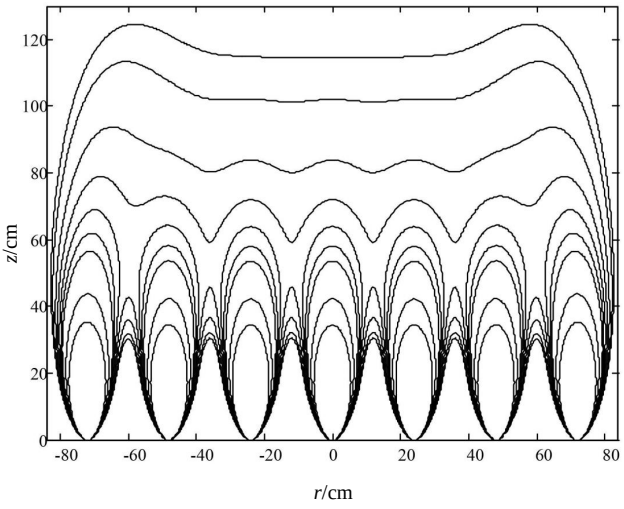

Figure 10: Constant-velocity body in the multiple-drawpoints draw process.

4.3 Constant-velocity body in ore particles drawn from multiple drawpoints

According to the definition of traditional draw theory, a constant-velocity body is one whose vertical descent rate is constant [25]. A constant-velocity body can be illustrated based on Equation (3). The body is shown in Figure 10.

Figure 10 shows that the constant-velocity body is symmetrical with respect to the bus of the No. 4 drawpoint, which forms the shape of a complete ellipsoid in the lower part of the model. The constant-velocity body of the No. 1 and No. 7 drawpoints occurs toward the middle of the model and the shape is slightly larger than it is at the centre. In the middle and upper parts of the model, the constant-velocity ellipsoids intersect each other. The wave form is higher on both sides and lower in the middle and this fluctuation is smaller closer to the top.

5 Correlations between flow patterns and velocity fields

The marked particles in each layer had a quasi-linear morphology at the top of the physical model. In the lower part of the model, the amplitude of the layers was greater and they showed an undulating morphology. This phenomenon is similar to the results obtained using vertical

velocity. The horizontal direction was used to determine which drawpoint the particles came from; therefore, under the influence of the side wall, the distribution of thirteen concentric points in each layer readily illustrates that the ore particles drawn from each drawpoint came from the centreline between it and the adjacent drawpoint. The horizontal and the vertical velocities of drawpoints No. 1 and No. 7 were greater than the velocities of the other five drawpoints. The minimum vertical velocity was found near the side wall and the maximum horizontal velocity deviated from the side wall, which brought the draw column of drawpoints 1 and 7 close to the middle of the model. It is quite possible that the stack ore velocity close to the side wall of the model at drawpoints No. 2 and No. 6 were greater since both the horizontal and vertical velocities in drawpoints No. 1 and No. 7 were greater than at other drawpoints. Wall friction had no influence on the flow of ore above drawpoints No. 2 and No. 6; hence, the ore decreased fastest in this part and the arrangement of marked particles in each layer were concave. Because the barrier was on the surface of the ore, its morphology was similar to that of the ore; their indirect contact resulted in the lowest depression of the barrier, as demonstrated by this experiment.

Figures 4 and 10 show that, in the multiple-drawpoints draw test, there was a similar relationship between the constant-velocity body and the draw column. Both formed complete ellipsoids in the lower part of the model and fluctuating curves in the upper part. The constant-velocity body coincided with the release body; this phenomenon reveals the essence of the morphology evolution of the draw column.

6 Discussion

The velocity field of ore particles is the basis of determining their motion trail and the morphology of the draw column, and it is one of the core contents of draw theory. Based on classical draw theory and considering the influence of a flexible barrier, the flow low and the velocity field equations of ore particles and the correlation between them with multiple drawpoints were studied. This study is not only helpful to clarify the flow law and its mechanism of ore particles under the influence of a flexible barrier, but also can enrich the draw theory, which has certain academic significance and practical engineering significance.

The main feature of the method of mass draw and synchronous filling with no-top-pillar shrinkage stoping is that a flexible barrier is laid on the surface of an ore pile before drawing the ore. In the process of drawing, filling materials are filled into the stope room through the return airway in a timely fashion and the filling materials and ore particles sink synchronously and uniformly. In this way, the stability of surrounding rock can be controlled and the ore loss and dilution can be reduced. In this paper, the flow law of ore particles in the mass draw and synchronous filling process is explored by physical experiments, and the velocity field equation of the ore particles through multiple drawpoints under the influence of a flexible barrier is established by theoretical derivation. The research results show that the flow law of ore particles is highly consistent with the distribution results of the velocity field of ore particles, which is similar to the research results of Tao [14], Castro [15, 16] *et al.* in the caving method.

However, at present, there are few experimental studies on the flow law of ore particles through multiple drawpoints. The draw theory established in this paper lacks practical examination, and its mathematical model is still far from being used to guide the production of mines. In the future, it needs to be further verified and adjusted with field measurement and laboratory research.

7 Conclusions

(1) Through a physical simulation experiment of the synchronous filling mining method, we found that the discharge amount at each drawpoint per unit time is approximately equal. This can be used as an important theoretical basis to study the velocity superposition effect of ore particles through multiple drawpoints under the influence of a flexible barrier.
(2) The velocity field analysis results for ore particles through multiple drawpoints under the influence of a flexible barrier were highly consistent with the flow properties of ore particles in the physical test.
(3) The shape of the draw column is essentially determined by the flow velocity of the ore particles. Therefore, the shape of the draw column can be determined by the velocity field equation of the ore particles in production practice; hence, the stope structure parameters can be designed and optimized.

Acknowledgement: This work was supported by the National Natural Science Foundation of China (Grant No. 51464005).

References

[1] Liu Y., Guo L., Ren Z., The causes of land landscape changes in semi-arid area of Northwest China: a case study of Yulin city. Journal of Geographical Sciences, 2006, 16, 192-198

[2] Long R., Zhang X., Negative entropy mechanism of the circular economy development countermeasures in mining area. Procedia Earth & Planetary Science, 2009, 1, 1678-1685

[3] Bian Z., Yang H., Daniels J., Frank O., Sue S., Environmental issues from coal mining and their solutions. International Journal of Mining Science and Technology, 2010, 20, 215-223

[4] Milanez B., Oliveira J., Innovation for sustainable development in artisanal mining: Advances in a cluster of opal mining in Brazil. Resources Policy, 2013, 38, 427-434

[5] Chen Q., Wu Z., A large number of ore drawing synchronous filling no-top-pillar shrinkage stopping method. CN, 2010

[6] Chen Q., Chen Q., Synchronous filling mining technology idea and a kind of representative mining method. China Mining Magazine, 2015, 24, 86-88

[7] Chen Q., Chen Q., Zhong J., Flow pattern of granular ore rock in a single funnel under a flexible barrier. Chinese Journal of Engineering, 2016, 38, 893 -898

[8] Chen Q., Zhao F., Chen Q., Wang Y., Zhong Y., Niu W., Orthogonal simulation experiment for flow characteristics of ore in ore drawing and influencing factors in a single funnel under a flexible isolation layer. JOM, 2017, 69, 2485-2491

[9] Chen Q., Chen Q., Zhong J., Chen D., Li S., Niu W., Evolution law of interface morphology of flexible isolation layer under ore drawing from single funnel. The Chinese Journal of Nonferrous Metals, 2016, 26, 6, 1332-1338

[10] Rustan A., Gravity flow of broken rock-what is known and unknown. In: Proceedings of MassMin 2000, Brisbane, Australia, 2000, 557-567

[11] Brown E., Block caving geomechanics. The international cavingstudy stage I-1997 through 2000. The University of Queensland, Australia, 2003.

[12] Kuchta M., A revised form of the Bergmark-Roos equation for describing the gravity flow of broken rock. Mineral Resources Engineering, 2002, 11, 4, 349-360

[13] Melo F., Vivanco F., Fuentes C., Apablaza V., On drawbody shapes: From Bergmark-Roos to kinematic models. International Journal of Rock Mechanics & Mining Sciences, 2007, 44, 1, 77-86

[14] Tao G., Ren Q., Ma J., Ore drawing rules produced by poly-drawpoints based on kinematic model. Journal of China coal society, 2012, 37, 3, 407-410

[15] Castro R., Trueman R., Halim A., A study of isolated draw zones in block caving mines by means of a large 3D physical model. International Journal of Rock Mechanics and Mining Sciences, 2007, 44, 6, 860-870

[16] Truemana, R. Castro R., Halim A., Study of multiple draw-zone interaction in block caving mines by means of a large 3D physical model. International Journal of Rock Mechanics and Mining Sciences, 2008, 45, 7, 1044-1051

[17] Kvapil R., Gravity flow of granular material in hoppers and bins. International Journal of Rock Mechanics and Mining Sciences, 1965, 2, 1, 35-41

[18] Vivanco F., Watt T., Melo F.L, The 3D shape of the loosening zone above multiple draw points in block caving through plasticity model with a dilation front. International Journal of Rock Mechanics and Mining Sciences, 2011, 48, 3, 406-411

[19] Meloa F., Vivancoa F., Fuentes C., Apablaza V., Kinematic model for quasi static granular displacements in block caving: Dilatancy effects on drawbody shapes, International Journal of Rock Mechanics and Mining Sciences, 2008, 45, 2, 248-259

[20] Wang J., Zhang J., Song Z., Three-dimensional experimental study of loose top-coal drawing law for longwall top-coal caving mining technology. Journal of Rock Mechanics and Geotechnical Engineering, 2015, 7, 3, 318-326

[21] Yang Q., Liu X., Drawing of caving ore block. Metallurgical Industry Press, Beijing, 1958

[22] Ren F., Theory and application of random medium ore drawing. Metallurgical Industry Press, Beijing, 1994,1-77

[23] Mullins W., Nonsteady W., State particle flow under gravity an extension of the stochastic theory. Appl.Mech, 1974, 41, 4, 867-872

[24] Chen Gang., Stochastic Modeling of Rock Fragment Flow Under Gravity. International Journal of Rock Mechanics and Mining Sciences, 1997, 34, 2, 323-331

[25] Qiao P., Ren F., The movement density field and velocity field of blasted ore-rock materials, China Mining Magazine, 2004, 13, 55-57